Cement & Concrete Composites 32 (2010) 810–818

Contents lists available at ScienceDirect

Cement & Concrete Composites

journal homepage: www.elsevier.com/locate/cemconcomp

Behaviour of Strain-hardening Cement-based Composites (SHCC) under monotonic and cyclic tensile loading
Part 2 – Modelling

Petr Jun, Viktor Mechtcherine *

Institute of Construction Materials, TU Dresden, D-01062 Dresden, Germany

ARTICLE INFO

Article history:
Received 8 February 2010
Received in revised form 29 June 2010
Accepted 30 July 2010
Available online 11 August 2010

Keywords:
SHCC
Constitutive relations
Multi-scale modelling
Cyclic behaviour

ABSTRACT

Following the presentation of experimental work in Part I of this article [1] the present part is dedicated to the derivation of constitutive relations for Strain-hardening Cement-based Composites (SHCC) under monotonic and cyclic tensile loading. These constitutive relationships are developed on the basis of a multi-scale modelling approach which considers the determining physical phenomena observed in experimental investigations. The multi-scale model is based on reproducing the fibre-pullout behaviour under monotonic as well as under cyclic loading by a multi-linear approximation, while statistics are used to describe the variation of results as observed in the experiments. Fibre embedment length and inclination serve as main parameters. These responses are further superimposed in order to describe the stress-crack opening behaviour of each individual crack while being loaded, unloaded, or reloaded. The overall stress–strain relationships for material under tensile loading are then derived by considering an increasing number of serial cracks and the contribution of the uncracked matrix. Particular cracking behaviour is adjusted by varying the model parameters. The modelled tensile behaviour of the material is compared with representative results of uniaxial tensile tests performed on the investigated SHCC, and the results of this comparison are discussed.

1. Introduction

This article regards the modelling of Strain-hardening Cement-based Composites (SHCC), which display high strain capacity when subjected to tensile loading. This ductile behaviour results from progressive multiple cracking achieved by the optimised crack-bridging action of short, thin, well distributed polymeric fibres.

Behaviour of the SHCC investigated under monotonic and cyclic tensile loading was described in Part I of this paper [1]. Furthermore, the experimental investigation performed on single fibres and single-fibre-pullout behaviour was presented. As was shown the stress stress–strain behaviour observed at the macro-level, where the material can be assumed to be homogeneous, depends on a number of micromechanical mechanisms. Therefore, a multi-scale approach is needed in order to comprehend the material behaviour observed and to develop a sound physical material model as a basis for a material law.

Several research projects have proposed different modelling approaches for SHCC subjected to tensile loading. Han et al. [2] and Vorel and Boshoff [3] introduced the constitutive relations for SHCC based on the reproduction of experimental results obtained from the tests on bulk SHCC specimens. The derived formulas are adequate for use in structural analysis. However, the approach does not enable the analysis of the mechanisms of material deformation behaviour and failure depending on the specific microstructural properties.

For representative volume elements of the material, Kabele [4] defined the stress vs. strain relationship, which considered micromechanical phenomena and further employed spatial averaging in order to link the scales of observation. He used the fibre-pullout description according to Lin et al. [5].

In this paper, the analytical model based on a multi-scale modelling approach is introduced. The pullout behaviour of individual fibres is modelled by multi-linear approximation of the experimental results while using statistics in order to describe the variance observed in the experiments. Fibre embedment length and inclination serve as the main parameters. The stress-crack-opening relationship for the individual cracks is derived from the concerted action of fibres involved in crack bridging. Subsequently, the joint response of individual cracks interconnected in series and the contribution of the uncracked matrix resulted in the overall stress–strain response of SHCC exposed to tensile loading. This last step

* Corresponding author. Tel.: +49 351 463 35 920; fax: +49 351 463 37 268.
E-mail address: mechtcherine@tu-dresden.de (V. Mechtcherine).

0958-9465/$ - see front matter © 2010 Elsevier Ltd. All rights reserved.
doi:10.1016/j.cemconcomp.2010.08.004

is similar to the approach used by Fischer [6] in the case of monotonic tensile loading; however, the constitutive relations which he used for the description of the single-crack behaviour were derived directly from the tension test on notched prisms.

2. Basis for material modelling

The experimental results presented in [1] demonstrated that the fibre pullout process, determined by the properties of the interface between the fibre and matrix, is the governing phenomenon in respect of the composite performance under monotonic and cyclic tensile loading. A series of fibre pullout tests in monotonic and cyclic regime provided the information needed to describe the material behaviour [1]. However, due to the inevitable limitations of the pullout apparatus, experimental investigations on fibre-pullout behaviour do not directly reflect the real pullout behaviour of the fibres crossing a crack in SHCC. The main aspects to be addressed in this regard are: (1) the effect of free fibre length needed to be set between the embedded and glued fibre ends on measured fibre pullout displacements; (2) the effect of fibre declination from the direction perpendicular to the matrix surface on its pullout behaviour; and (3) the fact that only single-side pullout is tested in the corresponding experiments, while in reality partial delamination and even pullout of fibre on both sides of a crack may occur.

The current chapter describes the adjustment of the results obtained from pullout experiments necessary to enhance the significance of the pullout data with regard to modelling. Subsequently, the current chapter presents information on assumed fibre distribution in the composite and on fibre pullout characterisation in use.

2.1. Consideration of the free fibre length deformation in the pullout test

As was shown in [1], a free fibre length of 5 mm between its embedded and glued ends influenced the overall deformation development during the pullout tests. Since the deformation of the fibre itself is known from the tensile tests performed on single fibres, it can be subtracted from the deformation values measured in the pullout tests. The fibre deformation to be subtracted δ_s depends on the force level and can be estimated by Eq. (1), which was derived on the basis of single fibre tests:

$$\delta_s = 0.59 \cdot \delta_t(P) + 0.41 \cdot \delta_t(P_h) \tag{1}$$

where $\delta_t(P)$ = actual deformation as a function of actual force P, P_h = highest force related to the point where softening or unloading starts.

Eq. (1) takes into account that the total deformation of fibre consists of an elastic and a plastic component. The percentage of these two components related to the total deformation was found to be 59% for the elastic and 41% for the plastic component, respectively. When the force increases, the actual force P is equal to the highest force P_h at each point. As a result, the total fibre free length deformation (100%) is subtracted as a function of the force reached. In the case of softening or unloading (for cyclic loading), the contribution of the elastic deformation decreases with decreasing actual force, while the plastic deformation component remains constant as defined for the highest force P_h reached before load decrease.

2.2. Fibre distribution in the composite

Three-dimensional, random distribution of fibres in SHCC is considered; no wall effect is taken into account. Based on this assumption, the probability-density functions for the distribution of fibres embedded lengths and inclinations can be derived according to Li et al. [7] using Eqs. (2) and (3):

$$p(z) = \frac{2}{L_f} \quad 0 \leqslant z \leqslant \frac{L_f}{2} \tag{2}$$

where $p(z)$ = probability-density function of variable z, z = distance between centre of the bridging fibre and the crack surface, L_f = fibre length;

$$p(\phi) = \sin\phi \quad 0 \leqslant \phi \leqslant \frac{\pi}{2} \tag{3}$$

where $p(\phi)$ = probability-density function of variable ϕ and ϕ = fibre inclination to the perpendicular to the crack plane.

Eq. (2) implies that the distribution of the fibres' embedded lengths along the crack is constant, i.e. each particular embedded length from the possible range has the same probability of participation in crack-bridging action as any other. Eq. (3) shows that the distribution of fibres with respect to their inclinations is determined by a sine function. The assumption adopted determines the fibre inclination at one end located in the centre of an imaginary hemisphere base and the second end on the surface of this hemisphere. Therefore, the probability that the fibre is going to be oriented perpendicularly to the crack plane ($\phi = 0$) is the lowest. The probability increases with inclination approaching the parallel orientation of the fibre ($\phi = \pi/2$) to the crack. Further details can be seen in Fig. 1.

Furthermore, according to [7] Eq. (4) can be used for estimating the number of fibres N_f involved in crack bridging:

$$N_f = \frac{A_c V_f}{2A_f} \tag{4}$$

where A_c = cross-sectional area, V_f = fibre volume fraction in the composite, and A_f = fibre cross-sectional area.

The estimation using Eq. (4) was confirmed by visual inspection of SHCC fracture surfaces. For SHCC under investigation there are approximately 1000 fibres bridging 1 cm^2 of the crack surface in projection.

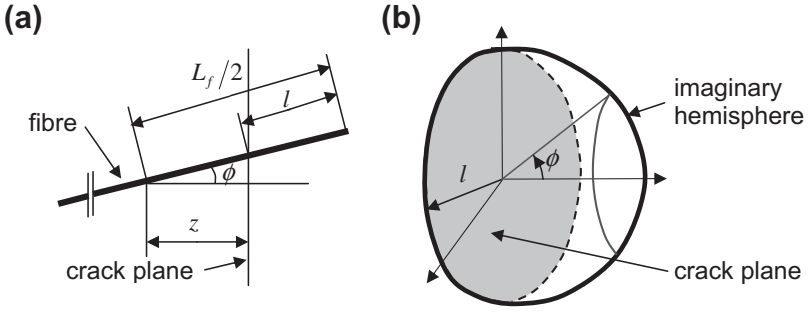

Fig. 1. Distribution of fibres according to Li et al. [7] with respect to: (a) embedded lengths and (b) inclinations to the crack plane.

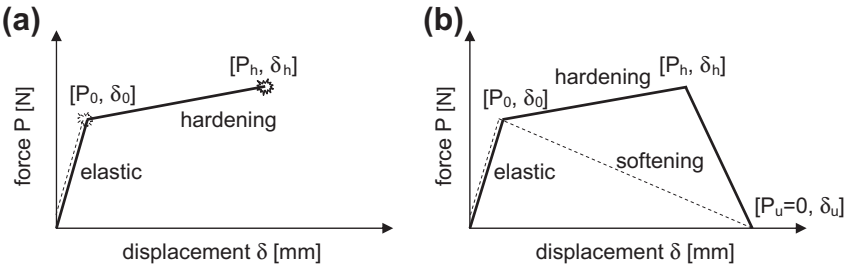

Fig. 2. Schematic presentations of force–displacement curves describing fibre-pullout behaviour: (a) fibre broken before de-bonding (thin dashed line) and after hardening (bold line) and (b) fibre pulled out in softening (thin dashed line) and hardening regime (bold line).

2.3. Defining the typical pullout responses

Four basic modes could be observed in the single-fibre pullout tests: (1) fibre fails before the de-bonding from the matrix is completed; (2) fibre fails after de-bonding and, as a consequence of fibre damage caused by friction with the inhomogeneous matrix during the hardening regime; (3) fibre is pulled out after slip hardening; and (4) fibre is pulled out after complete de-bonding of fibre from the matrix (no slip hardening occurs). In very rare cases the fibre failed in the softening regime after undergoing hardening. This scenario was not considered in respect of the modelling.

All measured force-to-displacement curves were divided into four groups according to the failure scenarios described above. The curves were subsequently approximated by linear or multi-linear plots, which were built by connecting characteristic points. The number and position of these points depend on a failure scenario: the first point was always the respective curve's origin (force = 0, displacement = 0). In describing the case of fibre failure before complete de-bonding, only one additional point is needed to indicate the force and deformation at failure. Three points were used to describe the response of fibres broken during hardening or the fibre pulled out after softening. Four points were needed to describe the response of fibres pulled out after hardening. Schematic pullout responses are given in Fig. 2.

The upper and lower limits of the force and displacement values were defined for each group of characteristic points. Because of the limited experimental data for different embedded lengths and the high variation of the pullout tests' results, it was not possible to determine clearly the statistical distribution of the values. An uniform probability distribution within the chosen intervals for force and displacement was therefore used at this stage, which is sufficient for the development of a modelling framework.

3. Derivation of constitutive relations at micro-level

3.1. Pullout response under monotonic loading

As explained in Section 2.3, pullout responses were described by using a number of linearly interconnected characteristic points. Fig. 2a shows a schematic response for the case of fibre rupture before de-bonding (one line) and fibre rupture after hardening (two lines). Fig. 2b shows the responses of fibres fully pulled out in the softening (two lines) and hardening regime (three lines).

Eq. (5) give a functional description of the single-fibre pullout model for all defined failure modes:

$$P = \begin{cases} k\delta & 0 \leqslant \delta \leqslant \delta_0 \\ P_0 + (P_h - P_0)\left(\frac{\delta-\delta_0}{\delta_h-\delta_0}\right) & \delta_0 \leqslant \delta \leqslant \delta_h \\ P_h\left(1 - \frac{\delta-\delta_h}{\delta_u-\delta_h}\right) & \delta_h \leqslant \delta \leqslant \delta_u \\ 0 & \delta_u \leqslant \delta \end{cases} \quad (5)$$

where k = fibre stiffness = $E * A_f$, E = fibre modulus of elasticity, A_f = fibre cross-sectional area; other characteristics are given in Fig. 2.

Based on this description and knowing the number of bridging fibres, the pullout responses can be generated within the given ranges using the uniform probability distribution. The number of responses generated for each specific failure scenario reflects the percentage of corresponding responses in the experimental investigation. Fibre responses are generated only for a representative unit crack plane area of 1 cm^2 in order to limit the computation time. It was proven that this simplification does not influence the prediction of the material behaviour on the meso-level when larger cracked cross-sections are considered.

3.2. Extension of the pullout results

Because of the limitations of the pullout test setup used, the effect of fibre inclination could not be studied directly. During fibre pullout the declination from the vertical results in increased friction of the fibre at the edge of the cracked matrix. In order to consider the effect of fibre inclination, the approach according to Kanda and Li [8] was adopted. According to this approach the enlargement of the pullout force due to an increased friction at the edges of the cracked matrix can be accounted for by using Eq. (6):

$$P_\phi = P_{\phi=0} \cdot e^{f\phi}, \quad f = 0.5 \quad (6)$$

where P_ϕ = enhanced pullout force as a function of fibre inclination ϕ, $P_{\phi=0}$ = pullout force for perpendicular direction to the crack plane, f = parameter determined from pullout experiments under different inclinations by [8].

However, when the friction increases locally, the fibre tends to fail earlier because of the resultant additional damage. Therefore, the fibre load-carrying capacity is limited to a maximum value according to Eq. (7):

$$P_{fu} = P_{fu}^n \cdot e^{f'\phi}, \quad f' = 0.3 \quad (7)$$

where P_{fu} = fibre maximum load-carrying capacity, P_{fu}^n = original load-carrying capacity (for fibre pullout perpendicular to the crack plane), ϕ = fibre inclination and f' = parameter determined by [8].

For all fibre responses, the inclinations are generated according to Eq. (3). Subsequently, the maximum pullout forces are increased according to Eq. (6) and, simultaneously, the fibre maximum load-carrying capacity is corrected, creating upper boundaries for fibre responses to be generated.

The last extension of the results is related to double-side de-bonding; see Wang et al. [9]. Pullout tests describe only single-side fibre de-bonding and pullout behaviour. However, in SHCC fibres can be partially or fully de-bonded from both sides of the crack. According to this phenomenon, the pullout deformation, before the failure is localised to one fibre end, is multiplied by 2. The

softening branch is then only moved to the new origin at a higher displacement, while its slope remains the same.

3.3. Generated pullout responses

Fig. 3 shows a number of the generated responses of fibres broken or pulled out in the specific modes described above. Extensions described in Section 3.2 are introduced here already. These extensions led partly to considerable changes in the failure mode. Due to the introduction of fibre inclination, and the related increase in the maximum pullout force accompanied by a decrease in fibre maximum load-carrying capacity, some fibres changed their specific pullout mode. The change in the pullout failure mode can be seen in the responses of fibres which would be otherwise partially or fully de-bonded and would undergo hardening or softening failure modes, cf. Fig. 3b–d.

3.4. Cyclic behaviour

Fig. 4 shows unloading–reloading loops extracted from a force–displacement diagram obtained in a cyclic fibre pullout test (cf. [1]). The figure also contains a simplified linear description of the loops. At the beginning of unloading, the pullout response typically shows a slight increase in deformation, which might result from pullout creep. At the beginning of the reloading a reverse tendency could be observed, i.e. a slight decrease in the measured displacement. These time-dependent components are, however, insignificant for the test rate used and therefore can be neglected. Loops are described by four points connected by straight lines. Three parameters are used to define a loop. The first defines the descent from maximal force while the displacement remains constant (the descent from point 1 to 2 in Fig. 4). The second parameter gives the displacement decrease due to unloading (from point 2 to 3 in Fig. 4). And finally, the third parameter defines the increase in force in the reloading regime without a change in displacement values (from point 3 to 4 in Fig. 4).

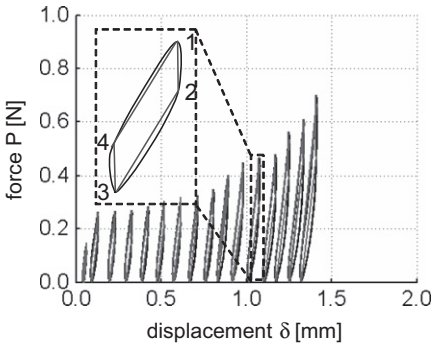

Fig. 4. Unloading–reloading loops from cyclic pullout tests and model description of the loops by four straight lines.

These three parameters are defined for each force level reached and approximated by linear functions by employing the method of least squares. Based on the linear dependencies observed, the shapes of the loops are defined as a function of the force reached. This procedure is further used to describe the cyclic fibre-pullout behaviour.

4. Derivation of the constitutive relations on meso-level

The formation and opening of merely one crack among many in SHCC is regarded as representative for the material behaviour at the meso-level. The modelling approach presented assumes that a crack is formed suddenly, through the entire cross-section, and in a direction perpendicular to the loading direction. Furthermore, it is assumed that one fibre can bridge only one crack. In reality, fibres can clearly bridge more than one crack. Therefore, the newly

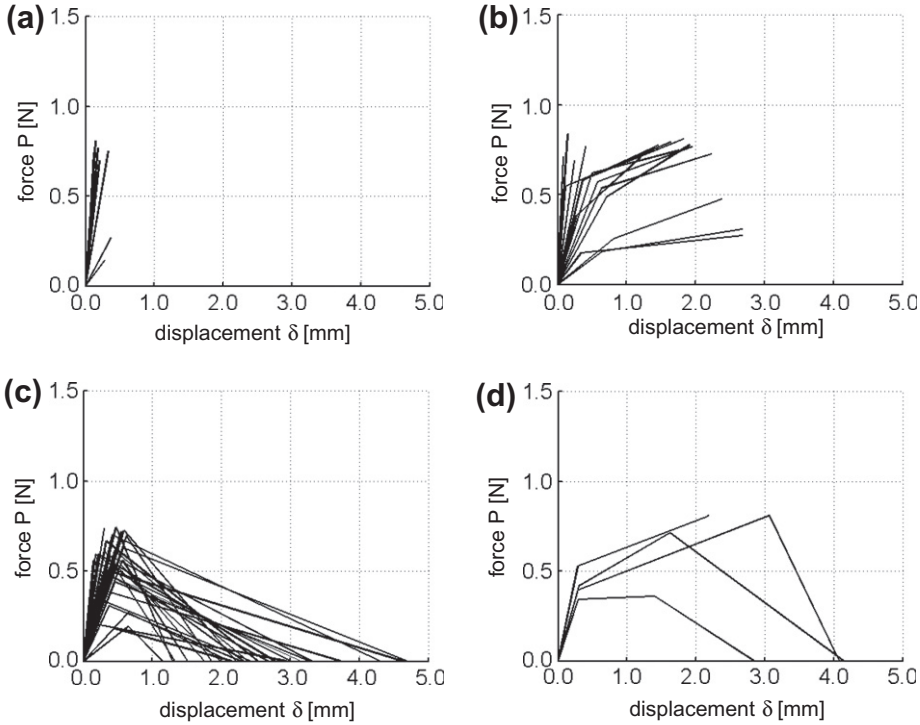

Fig. 3. Pullout responses generated for: (a) fibres broken before de-bonding, (b) fibres broken after partial or full de-bonding in the hardening process, (c) fibres fully de-bonded and pulled out in the softening process, and (d) fibres fully de-bonded and pulled out in the hardening process.

developed crack is not necessarily bridged by fibres fully bonded in the matrix, but some of them might be de-bonded and being pulled out already. This phenomenon is not considered in the model.

A stress-displacement curve giving a characteristic material response at this level of observation can be derived by adding the force contributions of all fibres bridging the crack using Eqs. (8) and (9):

$$P = \sum_{i=1}^{n} P_i(\delta_i) \tag{8}$$

where P = crack bridging force, P_i = carrying force of ith fibre as a function of displacement δ_i, and:

$$\sigma = \frac{P(\delta)}{A} \tag{9}$$

where σ = tensile stress, A = cross-sectional area of tensile specimen.

Fig. 5a shows a representative stress-displacement relation for monotonic tensile loading obtained using the procedure described above. The stress-displacement relation is within expected limits with respect to the tensile characteristics of the investigated SHCC (cf. [1]). By varying the number of fibres involved in crack-bridging action, the single-crack behaviour can be varied. However, no experimental evidence exists as yet to verify the shape of the curve directly. The assumption that tension tests on notched specimens provide the characteristic behaviour for one crack does reflect reality since in notched specimens made of SHCC more than one crack always develops [10]. Therefore, at the present state of knowledge, a constitutive relationship for the entire tensile specimen has first to be derived and subsequently compared with the corresponding experimental results obtained from uniaxial tension tests on dumbbell shaped specimens in order to evaluate the accuracy of the model.

Fig. 5a presents an approximation function for the modelled stress-displacement relation according to Eq. (10) as well. Such a formula is easier to handle when the contribution of many individual cracks to the SHCC bulk behaviour is considered.

$$\sigma = \gamma \cdot \beta \cdot \alpha^{-\beta} \cdot (\delta_l)^{\beta-1} \cdot e^{-\left(\frac{\delta_l}{\alpha}\right)^{\beta}} \tag{10}$$

where σ = actual tensile stress, α, β, γ = parameters, δ_l = crack opening deformation during loading (index l); the function is defined for $\delta_l > 0$.

The single-crack behaviour presented describes the theoretical opening of an individual crack which propagates through the entire cross-section but whose width remains infinitely low and is fully unloaded before further widening can start. This description results from the use of the pullout results as a basis for modelling and is characterised by describing the crack opening behaviour for stress levels starting at 0, i.e. for stress levels lower than those typically associated with crack formation. However, only that part of the stress-crack opening relationship after exceeding the particular matrix strength is relevant for the modelling of bulk SHCC.

The same approach as that used for the derivation of the stress-displacement relation for monotonic loading, i.e. superimposing the force contributions of all fibres involved in crack bridging of the crack under consideration (see above), is applied here also to determine the unloading and reloading branches during cyclic loading. Cyclic loops for individual fibres are created according to the force acting on an individual fibre at a given displacement level. The sum of all cyclic loops then creates the unloading–reloading response for one individual crack. Fig. 5b shows an example of calculated unloading and reloading loops for the displacements before unloading of 0.1, 0.2, 0.3, and 0.4 mm, respectively. The cyclic loops derived show similar behaviour for different stress levels of the stress-displacement relation. This can be traced back to the fact that the loops from pullout tests do not change their inclination or shape significantly with increasing displacement (cf. Fig. 4). The change in the inclination of loops observed on macro-level (i.e. for an unnotched specimen under tensile loading), see [1], results from an increasing number of cracks with increasing stress level, see Section 6.

The thin dashed line in Fig. 5b shows the course of the cyclic loops as described by an approximation function according to Eq. (11). Again, the reason behind introducing this equation is to simplify the handling of formulas when the contribution of many individual cracks to the SHCC bulk behaviour is considered.

$$\sigma = \sigma_{max}(\delta_{u,r})^{a} \tag{11}$$

where σ = actual tensile stress, σ_{max} = maximal stress before unloading, $\delta_{u,r}$ = unloading (index u), reloading (index r) deformation, a = parameter.

In order to fit the parameter "a" of Eq. (11), the original displacements were scaled to the non-dimensional interval from 0 to 1 and subsequent fitting was performed using the method of least squares. As a result, the stress function describing all unloading and reloading curves, respectively, could be defined. One value of parameter "a" was used for unloading and yet another for the reloading curves. The levels of the maximal stress reached were different for each particular loop. The original displacements were then used in conjunction with the obtained stresses, see Fig. 5b.

5. Derivation of constitutive relations for bulk material

5.1. Behaviour under monotonic loading

The overall stress–strain relationships for SHCC under tensile loading result from individual contributions of serially interconnected cracks and the contribution of the uncracked matrix. The

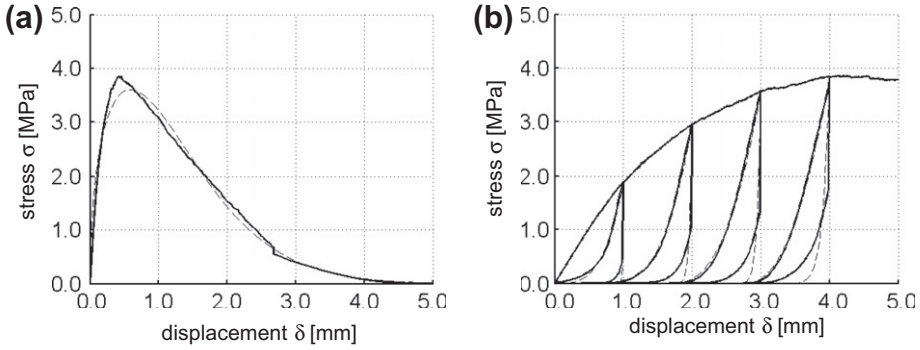

Fig. 5. Modelled single-crack behaviour (bold line) and its approximation (thin dashed line) for: (a) monotonic loading and (b) unloading and reloading in a deformation-controlled cyclic regime.

modelling approach presented for bulk material is similar to the framework introduced by Kabele [4]. However, different descriptions of pullout behaviour as well as of single-crack behaviour are used in this work. Furthermore, the cyclic behaviour is not considered in [4]. For modelling purposes the behaviour of the uncracked matrix is considered to be linear-elastic, i.e. no irreversible deformations are involved. The matrix strength at the points of the prospective crack formation is randomly generated using a uniform probability distribution in the value range provided by experimental results. Constitutive relations are derived under the condition of deformation control during loading, unloading and reloading.

The tensile response of SHCC can be subdivided into several stages. In the first stage, the material is loaded until the first-crack stress is reached. This stress level corresponds to the tensile strength of the weakest matrix cross-section. Since the behaviour of the uncracked matrix is considered to be linear-elastic, Eq. (12) is valid for unloading and reloading of the matrix as well:

$$\varepsilon_{l,u,r} = \frac{\sigma}{E} \tag{12}$$

where $\varepsilon_{l,u,r}$ = actual strain, l, u, r are indices for loading, unloading and reloading stage, σ = actual tensile stress, E = modulus of elasticity.

With the opening of the first crack, the fibres crossing the crack are activated; from this point they transmit the tensile stresses into the cracked cross-section. The crack then opens to some extent. Taking into consideration the condition of deformation control, the deformation immediately before and immediately after crack opening has to be the same. Therefore, the actual deformation of the specimen is equal to the sum of the unloading deformation of the matrix and the opening of the newly formed crack. Thus, this crack opening is determined by the unloading of the matrix, cf. Eq. (12), and by the stress-deformation curve for the crack, cf. Eq. (10). As a result of the steadily increasing deformation (deformation control), the overall tensile stress in SHCC drops with the opening of the first crack. The drop can be determined by solving the system of Eq. (13) using the Newton–Raphson method.

$$\begin{aligned} &-\sigma_{1,d}(\varepsilon_u) + \sigma_{1,d}(\delta_{1,l} = 0) \\ &-\varepsilon_u l_0 - \delta_{1,l} + \varepsilon_1 l_0 = 0 \end{aligned} \tag{13}$$

where $\sigma_{1,d}$ = stress after first drop, ε_u = unloading deformation of the matrix, $\delta_{1,l}$ = opening of the first crack, l_0 = gauge length of the specimen, ε_1 = actual deformation after the formation of the first crack.

As soon as the sudden stress drop is complete and the stress begins to rise again, the matrix deformation gradually increases as well. Simultaneously, the newly developed crack continues opening and contributes therewith to the overall deformation. Since the carrying capacity of the fibres bridging the crack is higher than the tensile strength of the matrix in the second weakest cross-section, the scenario carries on until this strength is reached. The corresponding increase in strain can be described by Eq. (14):

$$\varepsilon = \frac{\sigma}{E} + \frac{\delta_{1,j}(\sigma)}{l_0} \tag{14}$$

where ε = actual strain, σ = actual tensile stress, E = modulus of elasticity, $\delta_{1,l}$ = opening of 1st crack as a function of stress, l_0 = gauge length of the specimen.

When the matrix strength in the second weakest cross-section is reached, a new, second crack appears. Similarly to the situation after the formation of the first crack, the stress drops due to the new crack's opening. This drop in stress is determined as described above, with the difference that Eq. (13) must be extended in order to take into account the partial closing of the first crack. In general, the ith drop associated with formation of ith crack is determined by the unloading deformation of the matrix and $(i-1)$ cracks and by the opening of the ith crack. This results not only in an increasing number of members of the second equation given in Eq. (13), but in an increasing number of equations as well. For each additional crack opened one equation is added to the system in order to describe its closing during unloading when the next crack develops; $(i-1)$ equations are added in total. These additional equations are the same for each developed crack. The description for ith stress drop is given by Eq. (15):

$$\begin{aligned} &-\sigma_{i,d}(\varepsilon_u) + \sigma_{i,d}(\delta_{i,1}) = 0 \\ &-\varepsilon_u l_0 - \delta_{i,l} + \varepsilon_i l_0 - \sum_{1}^{i-1} \delta_{i,u} = 0 \\ &-\sigma_{i,d}(\varepsilon_u) + \sigma_{i,d}(\delta_{1,u}) = 0 \\ &\vdots \\ &-\sigma_{i,d}(\varepsilon_u) + \sigma_{i,d}(\delta_{i-1,u}) = 0 \end{aligned} \tag{15}$$

where $\sigma_{i,d}$ = stress after ith drop, ε_u = unloading deformation of the matrix, $\delta_{i,l}$ = opening of ith crack, l_0 = gauge length of the specimen, ε_i = actual deformation after ith crack, $\delta_{i,u}$ = partial closing of ith crack, $\delta_{1,u}$ = partial closing of 1st crack, $\delta_{i-1,u}$ = partial closing of $(i-1)$th crack.

After each stress drop, the matrix deformation starts to increase again, and simultaneously the newly developed crack is being opened. In addition, all already existing cracks reopen according to Eq. (11). The re-opening as well as the closing of the existing cracks is a function of the original stress-crack opening displacement state of each crack involved before the stress drop occurred. This scenario continues until the previous maximum stress (equal to the matrix strength at the location of the last crack) is reached. From this point on, all developed cracks are being opened according to Eq. (10). The parameters of Eq. (10) differ for individual cracks, which bespeaks slightly different properties in each particular crack. The parameters are generated randomly using the uniform probability distribution. The ranges for the generation were first estimated based on the expert knowledge and further adjusted after comparing the modelled tensile responses with the experimental results. The overall strain can be described by Eqs. (16) and (17):

$$\varepsilon = \frac{\sigma}{E} + \sum_{1}^{i-1} \frac{\delta_{i,r}(\sigma)}{l_0} + \frac{\delta_{i,j}\sigma}{l_0} \tag{16}$$

$$\varepsilon = \frac{\sigma}{E} + \sum_{1}^{i} \frac{\delta_{i,r}(\sigma)}{l_0} \tag{17}$$

where ε = actual strain, σ = actual tensile stress, E = modulus of elasticity, $\delta_{i,r}$ = re-opening of ith crack, $\delta_{i,l}$ = opening of ith crack, l_0 = gauge length of specimen.

The formation of new cracks carries on until the strength of the next weakest cross-section is higher than the carrying capacity of fibres bridging the crack with the weakest fibre reinforcement. The failure is then localised due to the exclusive opening of this particular crack, while the stress level decreases. Eq. (18) describes the material behaviour after failure localisation:

$$\varepsilon = -\frac{\sigma}{E} - \sum_{1}^{i-1} \frac{\delta_{i,u}(\sigma)}{l_0} + \frac{\delta_{i,u}(\sigma)}{l_0} \tag{18}$$

where ε = actual strain, σ = actual tensile stress, E = modulus of elasticity, $\delta_{i,u}$ = partial closing of ith crack, l_0 = gauge length of the specimen, $\delta_{i,l}$ = opening of ith crack.

5.2. Behaviour under cyclic loading

SHCC behaviour under cyclic tensile loading is described in a way consistent with the material behaviour under monotonic tensile loading. When the unloading begins at a given strain level, matrix deformation starts to decrease according to Eq. (12) and all the developed cracks start to close following the Eq. (11). The particular shape of the unloading function for each developed crack depends on the original stress–strain state of this particular crack at the moment when the unloading begins. The principle of superposition is used in order to consider the deformation contributions. Behaviour of cracked SHCC during the unloading is given by Eq. (19):

$$\varepsilon = \varepsilon_o - \frac{\sigma}{E} - \sum_{1}^{i} \frac{\delta_{i,u}(\sigma)}{l_0} \tag{19}$$

where ε = actual strain, ε_0 = original strain, σ = actual tensile stress, E = modulus of elasticity, $\delta_{i,u}$ = closing of ith crack, l_0 = gauge length of the specimen.

The unloading continues until it reaches zero stress and a certain residual strain. Subsequently, the reloading which brings the material back to the original state can take place. Eq. (20) describes the cracked SHCC during reloading:

$$\varepsilon = \varepsilon_r + \frac{\sigma}{E} + \sum_{1}^{i} \frac{\delta_{i,r}(\sigma)}{l_0} \tag{20}$$

where ε = actual strain, ε_r = residual strain, σ = actual tensile stress, E = modulus of elasticity, $\delta_{i,r}$ = re-opening of ith crack, l_0 = gauge length of the specimen.

The modelling approach as derived at the micro-level does not consider any crack-closing resistance. This mechanism can be attributed to the friction at the crack edges due to loosened parts of the matrix. In considering this phenomenon an additional parameter R, which reduces the closing capacity of cracks, was used according to Eq. (21). The importance of crack-closing resistance to the overall unloading of the composite is higher, the higher the number n of cracks developed. The crack-closing resistance parameter reduces the unloading increments, and its value increases linearly as a function of the number of involved cracks. This modification obviously leads to a shift of a starting point of the reloading loop towards higher strain values.

$$R = 0.05n + 1.8 \tag{21}$$

where R = crack-closing resistance parameter, n = number of cracks.

Eq. (21) was obtained empirically by fitting the cyclic behaviour of SHCC as observed in the experimental investigations, see [1]. Crack resistance to closing is taken into account also in the description of failure localisation in the specimen where a number of cracks are being closed while the crack opens in the weakest cross-section. This phenomenon is however neglected when modelling the stress-dropping mechanism. Such simplification is appropriate due to insignificant unloading deformations associated with developed cracks at the stage immediately after beginning of unloading, see Fig. 5b, which is relevant for the stress-drop description.

6. Results of modelling and discussion

Fig. 6 shows examples of the modelled SHCC behaviour under tension together with the representative responses obtained from uniaxial, deformation-controlled, monotonic tensile tests as presented in [1]. Since the model generates the matrix strengths and the particular shapes of stress-crack opening relations randomly and anew every time it runs, each generated overall stress–strain response is different to some extent. The model does not prescribe the number of cracks initiated, the procedure runs automatically and the localisation occurs as soon as the corresponding criterion is satisfied. Therefore, the strain capacity and the tensile strength of each modelled curve are the predicted outputs, not the parameters prescribed. This approach enables the generation of original stress–strain relations within the limits chosen according to the experimental findings.

The stress–strain relations provided by the model meet quite well both quantitatively and qualitatively the representative curves obtained by experiments, cf. Fig. 6. With an appropriate choice of parameters, the first-crack stress and the tensile strength of the composite are in good agreement with the experimental results. However, in order to achieve correspondence of both experimental and modelled tensile strength values, the assumed behaviour of individual cracks related to the amount of bridging fibres was modified. The number of fibres N_f acting in the "weakest crack" was enlarged by 20% and for the "strongest crack" (i.e., the crack with the strongest crack bridging by fibres) by 40% related to the initially considered number of fibres in every cross-section. As explained above this number was estimated using Eq. (4) and further verified by means of the evaluation of microscopic images at some spots of the fracture surfaces. Since the material's performance under tensile load is primarily governed by the weakest link, the cracked cross-section with the weakest crack bridging determines the failure. The "degree of reinforcement" of cracks with higher carrying capacity influences the inclination toward the cracks' re-opening and opening branches after cracking and, hence, the strain capacity of the SHCC.

The single crack relations were generated to model the overall SHCC response within these enhanced limits. The need for enhancement can be explained, at least in part, by assuming a planar cracking surface as the basis for determining the fibres'

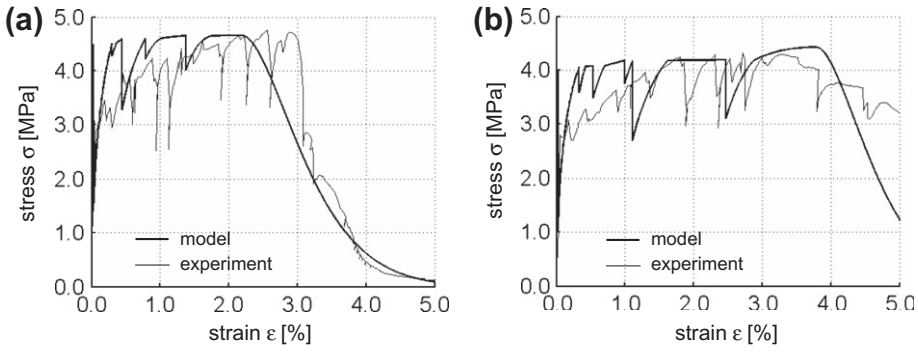

Fig. 6. Comparison of the modelled stress–strain relations for SHCC in tension under monotonic loading (bold lines) and representative experimental results (thin lines), parameters used for modelling were: (a) σ_1 = 4.5 MPa, N_f = 120–140% and (b) σ_1 = 4.0 MPa, N_f = 120–140%.

number. In the specimens tested, however, cracking surfaces were often found not to be planar but rather rough and not always exactly perpendicular to the specimen's longitudinal axis. Thus, the number of fibres bridging a particular crack and their combined carrying capacity are likely to be higher in reality. Furthermore, the approximation function used as the input stress-crack opening relation for each individual crack provides a slightly lower strength value (cf. Fig. 5a), which weakens the overall performance of the modelled material to some extent.

The curves obtained from the modelling reach approximately the same strain capacity as measured in the experiments but have fewer cracks in comparison to the number of cracks observed experimentally. The typical measured density of visible cracks going through the entire cross-section was slightly higher than one crack per centimetre in the case of small dumbbell specimens. For the gauge length used it meant approximately 12 cracks per specimen. However, the number varied between approximately 9 and 15 cracks for specimens at the ultimate strain. On examining the experimental curves more closely, approximately such number of evident "jumps", which indicate the formation of new cracks, can be noted. However, additional less pronounced "jumps" can be observed as well. These additional "jumps" are of small magnitude so that they likely correspond to formation of very fine, hardly visible cracks or cracks which penetrate only a part of the specimen cross-section.

Contrarily, the modelled relations indicate formation of only 5–6 cracks in these particular cases. Such cracking behaviour can be interpreted as if the opening of each modelled crack is accompanied by non-elastic deformations higher than those observed in the experiments. This finding is, again partially related to the approximation formula for the stress-deformation relations used as the input relation to model the overall material response. As can be seen in Fig. 5a, the approximation curve exhibits a more inclined (gentler) shape around the point of maximal stress. The peak also corresponds to a higher deformation level in comparison to the originally modelled crack opening relation. However, it can also be traced back to the more complex shape of the cracks observed in experiments. In such cases, the load-carrying capacity of the individual cracks increases with an increasing number of bridging fibres due to the higher fracture surface area. The pre-peak deformation of these cracks associated with stresses among the range of matrix strengths decreases due to a steeper inclination of the stress-crack opening relations.

The ongoing parametrical study will provide evidence as to whether these aspects are really important to the quality of the description of SHCC behaviour. In general, the modelled behaviour is determined especially by the difference between the first-crack stress and the load-carrying capacity of the weakest crack involved. If the difference is low, the modelled response is likely to predict only limited hardening and low strain capacity. On the other hand, if the difference is pronounced, significant hardening and high strain capacity are likely to occur. The modelled behaviour is further significantly influenced by the values of matrix strengths which determine the upper envelope shape of the modelled curves and by the opening of particular individual cracks which determine the strain capacity and number of cracks modelled.

The modelled cyclic behaviour compared quantitatively quite well with the experimental results obtained for SHCC under cyclic deformation-controlled tensile loading. A slight disagreement can be, however, observed for higher strain levels, i.e. above 2.5%. The comparison is shown in Fig. 7. The qualitative description, i.e. especially the shape of reloading branches, is, however, restricted due to the approximation used for single-fibre-pullout behaviour under cyclic loading. Cycles on the micro-scale are characterised by a significant ascent in the approximation approach when the reloading is introduced; see Fig. 4. However, this ascent is only significant as long as the scale of axis is considered. After adding the cyclic pullout responses to each other, the sudden ascent is no longer pronounced. It only results in a steeper slope of the reloading branch. Therefore, the characteristic slope of reloading branches known from the tensile tests on dumbbell specimens cannot be reproduced exactly by the model. The modelled convex shape of the curve can only be changed by choosing another approximation function at the microscopic level of observation.

Introducing the crack-closing resistance parameter R led to a reduction of the irreversible deformation. Fitting this parameter to the experimental results revealed a lower need to increase irreversible deformation at higher strain levels. The parameter R should therefore increase less markedly with an increasing number of cracks. This means that the formulation of Eq. (21) should be reconsidered. Further investigations, including the parametrical study, are needed in order to obtain more extensive knowledge of the mechanisms involved and to improve the model further.

7. Summary and concluding remarks

The work presented describes the development of a link between the microscopic and macroscopic levels of observation for a Strain-hardening Cement-based Composite and the subsequent development of a modelling framework for strain-hardening materials under monotonic and cyclic tensile loading. The constitutive relationships derived consider the specific physical phenomena investigated at different levels of observation.

The results of single-fibre pullout tests were used as the basis in modelling the material behaviour on the micro-level. Typical responses with the different failure modes obtained from the pullout

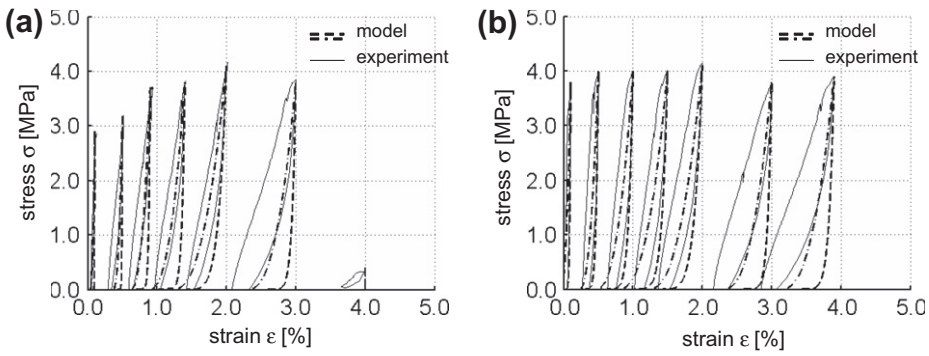

Fig. 7. Comparison of the modelled stress–strain relations for SHCC in tension under cyclic loading (bold lines) and representative experimental results (thin lines); dashed line stands for unloading, dash-and-dot line for reloading; only a few selected loops are shown.

tests were modelled by multi-linear relations, which subsequently were corrected in order to eliminate the effect of the test setup and extended to consider the effect of fibre inclination as well as of fibre de-bonding on both sides of a crack. As a result, a set of representative force–displacement relations for fibre-pullout behaviour, including the unloading and reloading regimes, was derived.

By superimposing the pullout responses of all fibres involved in the crack-bridging action, a stress-crack opening relationship for each individual crack could be obtained, including the unloading and reloading parts.

The stress–strain relations for bulk SHCC under monotonic and cyclic deformation-controlled tensile loading were developed based on the joint action of the uncracked matrix and gradually developing system of cracks in serial interconnection.

The model was verified by comparison of the predicted tensile responses under monotonic and cyclic loading with experimental results obtained from the uniaxial tensile tests on SHCC. In general the experimental and predicted curves were found to be in good agreement. However, the model will be further developed by better understanding and considering some specific material phenomena. This is the subject of the ongoing research work by the authors.

The outlined approach can be used, first of all, as an aid in the material design of advanced fibre-reinforced cement based materials like SHCC, but it also can provide a good basis for defining material laws suitable for design codes.

References

[1] Jun P, Mechtcherine V. Behaviour of Strain-hardening Cement-based Composites (SHCC) under monotonic and cyclic tensile loading; Part 1 – experimental investigations. Cem Concr Compos 2010;32(10):801–9.
[2] Han T-S, Feenstra PH, Billington SL. Simulations of highly ductile fiber-reinforced cement-based composite components under cyclic loading. ACI Struct J 2003;100(6):749–57.
[3] Vorel J, Boshoff WP. Numerical modelling of strain hardening fibre-reinforced composites. In: International conference on advanced concrete materials, ACM 2009. Stellenbosch, South Africa: Taylor & Francis Group; 2009. p. 271–78. ISBN 978-0-415-87637-7.
[4] Kabele P. Multiscale framework for modeling of fracture in high performance fiber reinforced cementitious composites. Eng Fract Mech 2007;74:194–209.
[5] Lin Z, Kanda T, Li VC. On interface characterization and performance of fibre reinforced cementitious composites. Concr Sci Eng 1999;1:173–84.
[6] Fischer G. Development of cracking in strain hardening cementitious composites, (SHCC). In: International workshop NMMF 2007, workshop proceedings. Wuppertal, Germany: Aedificatio Publishers; 2007. p. 151–62.
[7] Li VC, Wang Y, Backers S. A micromechanical model of tension-softening and bridging toughening of short random fiber reinforced brittle matrix composites. J Mech Phys Solids 1991;39(5):607–25.
[8] Kanda T, Li VC. Interface property and apparent strength of high-strength hydrophilic fiber in cement matrix. J Mater Civil Eng 1998;10(1):5–13.
[9] Wang Y, Li VC, Backers S. Modeling of fiber pull-out from a cement matrix. Int J Cem Compos Lightweight Concr 1988;10(3):143–9.
[10] Mechtcherine V, Jun P. Behaviour of strain-hardening cement-based composites in tension and compression – overview of recent research. In: Gettu R, editor. Seventh international RILEM symposium on fibre reinforced concrete: design and applications, RILEM Publications S.A.R.L.; 2008. p. 471–81.